

The dust properties of $z \sim 3$ MIPS-LBGs from photo-chemical models

X.L. Fan^{1,2,3,4}, A. Pipino⁵ and F. Matteucci^{3,4,6}

ABSTRACT

The stacked spectral energy distribution (SED) of Multiband Imaging Photometer for Spitzer (MIPS) $24\mu\text{m}$ detected Lyman break galaxies (MIPS-LBGs) is fitted by means of the spectro-photometric model GRASIL with an “educated” fitting approach which benefits from the results of chemical evolution models. The star formation rate-age-metallicity degeneracies of SED modelling are broken by using the star formation history and chemical enrichment history suggested by chemical models. The dust mass, dust abundance and chemical pattern of elements locked in the dust component are also directly provided by chemical models. Using our new “fitting” approach, we derive the total mass M_{tot} , stellar mass M_* , gas mass M_g , dust mass M_d , age and star formation rate (SFR) of the stacked MIPS-LBG in a self-consistent way. Our estimate of $M_* = 8 \times 10^{10}$ of the stacked MIPS-LBG agrees with other works based on UV-optical SED fitting. We suggest that the MIPS-LBGs at $z \sim 3$ are young (0.3-0.6 Gyr), massive ($M_{tot} \sim 10^{11} M_\odot$), dusty ($M_d \sim 10^8 M_\odot$), metal rich ($Z \sim Z_\odot$) progenitors of elliptical galaxies suffering a strong burst of star formation ($\text{SFR} \sim 200 M_\odot/\text{yr}$). Our estimate of $M_d = 7 \times 10^7 M_\odot$ of the stacked MIPS-LBG is about a factor of eight lower than the estimated value based on single temperature grey-body fitting, suggesting that self-consistent SED models are needed to estimate dust mass. By comparing with the Milky Way molecular cloud and dust properties, we suggest that denser and dustier environments and flatter dust size distribution are likely in high redshift massive star forming galaxies. These dust properties, as well as the different types of SFHs, can cause different SED shapes between high redshift star-forming ellipticals and local

¹fan@oats.inaf.it

²Hubei University of Education, 430205, Wuhan, Hubei, China

³Dipartimento di Fisica, Sezione di Astronomia, Università di Trieste, via G.B. Tiepolo 11, I-34131, Trieste, Italy

⁴I.N.A.F. Osservatorio Astronomico di Trieste, via G.B. Tiepolo 11, I-34131, Trieste, Italy

⁵Institut für Astronomie, ETH Zurich, 8093 Zurich, CH

⁶I.N.F.N., Trieste, Via Valerio 2, 34100, Trieste, Italy

star-burst templates. This discrepancy of SED shapes could in turn explain the non detection at submillimeter wavelengths, of IR luminous ($L_{IR} \geq 10^{12} L_{\odot}$) MIPS-LBGs.

Subject headings: galaxies: high redshift—galaxies: starburst—ISM: clouds—ISM: dust, extinction

1. Introduction

The last decade witnessed a tremendous increase in the knowledge of high redshift star forming galaxies. Large samples, obtained with different selection techniques (see Shapley 2011, for a review), yielded statistical information about masses (e.g. Erb et al. 2006b; Daddi et al. 2007), star formation rates and dust attenuation (e.g. Hopkins & Beacom 2006; Reddy et al. 2008, 2010), as well as metallicities (e.g. Erb et al. 2006a) for $z \simeq 2$ galaxies.

In a small subset of well studied objects, a more accurate determination of their chemical abundance pattern, dust depletion, kinematics, was possible, due to lensing magnification (e.g. Hainline et al. 2009) and deep integral field observations (e.g. Law et al. 2012; Gnerucci et al. 2011; Genzel et al. 2011).

Taken together, these observables shaped our view of $z = 2 - 3$ redshift star forming galaxies as relatively evolved systems, as witnessed by their metallicities (e.g. Erb et al. 2006a; Calura et al. 2009), whose star formation rates are high due to the availability of large gas reservoirs as opposed to mergers (e.g. Genzel et al. 2010; Rodighiero et al. 2011; Kaviraj et al. 2012).

Among the various methods, the Lyman Break Technique (Steidel & Hamilton 1993) was particularly successful in yielding insight into high redshift star forming galaxies. Lyman break galaxies (LBGs) are observed at different redshifts: $z \sim 1$ (Burgarella et al. 2007), $z \sim 1.4-2.5$ “BX” and “BM” (Steidel et al. 2004), $z \sim 3$ (Steidel et al. 2003), $z \sim 4,5,6$ (Vanzella et al. 2009) by means of the photometrical selection technique for rest-frame 912 Å Lyman-continuum discontinuity in a desired redshift interval. To infer the properties of stars, interstellar medium (ISM) and dust, LBGs have been studied in terms of stellar light, interstellar absorption lines and rest-frame UV continuum at $z \gtrsim 3$ (Steidel et al. 2003; Vihj et al. 2003). One of the best studied LBGs is the gravitational lensed LBG MS 1512-cB58 (hereafter cB58) at redshift $z = 2.7276$, which seems to be a young system undergoing rapid star formation and possibly destined to be an elliptical galaxy (Pettini et al. 2002). By means of cosmological hydrodynamical simulations, Davé et al. (2000) suggested that LBGs at $z \sim 3$ are the most massive galaxies at that epoch without ruling out the merger-induced star-burst galaxies contribution. Using a chemodynamical model, Friaca & Terlevich (1999) suggested that LBGs at $z \sim 3$ are the progenitors of present-day massive spheroids. Matteucci & Pipino (2002) and Pipino et al. (2011) suggested that LBGs at $z \sim 3$ can

be young small star forming elliptical galaxies by fitting the abundance pattern of cB58 by means of galactic chemical evolution models. The stellar population properties of LBGs at $z \sim 3$ are studied by Sawicki & Yee (1998); Papovich et al. (2001); Magdis et al. (2008, 2010a); Pentericci et al. (2010).

In the absence of accurate spectroscopic data available for large galaxy samples, the stellar properties, such as the age and stellar mass are estimated by spectral energy distribution (SED) fitting based on stellar population synthesis models where star formation history (SFH), metallicity and dust extinction are independent free parameters. Whilst some studies adopt a full treatment of radiative transfer (e.g. Takagi et al. 2003; Siebenmorgen & Krügel 2007; Rowan-Robinson 2012; Lo Faro et al. 2013), in most cases empirical attenuation laws are usually adopted to deconvolve the effect of the dust from the SED. This means that molecular cloud (MC) condition, and dust properties, such as dust mass, dust abundance and dust size distribution, are not directly studied. Only a few works attempt to fit the SEDs of LBGs from the UV to the IR (e.g. Magdis et al. 2010b, 2011). However, separate models are adopted in these works to fit the UV-optical and the IR parts of the SED. Furthermore, the dust temperature and mass are usually estimated by a grey body fitting, and the IR luminosity are usually estimated with template SEDs from an observational library. Whilst these assumptions might be justified as a necessary to explore *uncharted territory* and certainly provide a good zero order estimate of the relevant physical quantities (masses, SFRs), we believe that more sophisticated models should be adopted to understand the physical processes acting in high redshift star forming galaxies at a finer degree of detail.

To this purpose, in previous work (Matteucci & Pipino, 2001, Pipino et al., 2011), we focussed on the chemical abundance pattern of a well studied single LBG cB 58 (Pettini et al. 2000) and LBGs from two surveys: AMAZE (Maiolino et al. 2008) and LSD (Mannucci et al. 2009). We self-consistently derived the SFH and the dust properties for these high redshift LBGs. Here we want to address in detail the dust properties of $z \sim 3$ LBGs. In particular, we will make use of the stacked SED of Multiband Imaging Photometer (MIPS) $24\mu\text{m}$ detected LBGs (MIPS-LBGs) at $z \sim 3$ (Magdis et al. 2010b), since they allow for the first time an entire coverage from the UV to the radio wavelengths. MIPS-LBGs, per se, are not a special class of objects. However they are likely the most massive, most dust rich, most rigorously star forming LBGs at redshift $z \sim 3$, following a SFR-stellar mass relation with a similar slope to that found at redshift $z=1$ (Elbaz et al. 2007) and $z=2$ (Daddi et al. 2008), but a higher normalization factor (Magdis et al. 2010a). The inferred properties of the stacked MIPS-LBG SED will represent the average massive LBGs at redshift $z \sim 3$. The high SFR and infrared luminosity suggest that MIPS-LBGs should be detected at submm wavelengths. However, this occurs in a small fraction of cases (Chapman et al. 2000; Shim et al. 2007; Chapman & Casey 2009). This non detection far-IR counterparts of MIPS-LBGs could be caused by higher dust temperature, different dust spatial distribution and lower SFR in LBGs than in submillimetre galaxies (SMGs) (see discussion in Chapman et al. 2000; Rigopoulou et al.

2006; Magdis et al. 2010b). The self-consistent SED model combined with chemical model will allow us to investigate this issue in more detail.

In our approach (see details below), we study the properties of stellar population and ISM by the spectro-photometric model GRASIL (Silva et al. 1998). Parameter degeneracy is a problem for any galactic SED fitting (see reviews by Gawiser 2009; Walcher et al. 2011). Therefore, our self-consistent chemical evolution model (Pipino et al. 2011), which can reproduce most of the chemical properties of ellipticals of different mass, is adopted to reduce the degree of freedom as much as possible in our SED modelling by GRASIL. The combination of chemical evolution models and GRASIL has been already adopted by Schurer et al. (2009) to model SEDs of different morphological type galaxies using the chemical and dust evolution models from Calura et al. (2008).

In this article, we aim at: 1) deriving the dust mass, and 2) investigating dust composition, temperature and grain size distribution of MIPS-LBGs. We will also assess the robustness of previously derived galaxy masses and SFR, compare MIPS-LBGs with other $z \sim 3$ LBGs, confirm the nature of LBGs at $z \sim 3$ from previous chemical models, and try to solve the challenge of non detection far-IR counterparts of MIPS-LBGs. The paper is organized as follows: in Sect. 2, we describe our models and fitting approach; our results and discussions are presented in Sect. 3; and our conclusions are drawn in Sect. 4. Throughout the paper, we adopt a (0.7, 0.3, 0.7) cosmology.

2. The models

We combine the chemical evolution models for elliptical galaxies (Pipino et al. 2011) and the spectro-photometric model GRASIL (Silva et al. 1998) to model the SED of the stacked MIPS-LBG. The combination approach is fully described in Schurer et al. (2009) for galaxies of different morphological type. We direct the reader to above articles for equations and details. For the sake of convenience the two models will be briefly summarized in the next sections. In particular, the details of the our “fitting” approach will be described.

2.1. The chemical evolution model

The chemical abundance ratios versus metallicity are amongst the best indicators to constrain the SFH of a galaxy. However, there is no chemical data of the average MIPS-LBGs at $z \sim 3$ to constrain the SFH. We adopt the SFHs of elliptical models (Pipino et al. 2011), which have successfully reproduced the chemical abundance properties of normal ellipticals (see Pipino & Matteucci, 2004) as well as those of low mass LBGs at $z \sim 3$ (see Pipino et al. 2011, for detail).

In this way, the SFH, metallicity enrichment and dust evolution history of a galaxy are obtained from a self-consistent chemical evolution model. The impact of this assumption is reviewed in the discussion section.

In these models, both the infall and the star formation timescale are assumed to decrease with galactic mass, in order to reproduce the “chemical downsizing” (e.g. Thomas et al. 2005). The initial conditions for ellipticals allow for the formation by either collapse of a gas cloud into the potential well of a dark matter halo or, more realistically, by the merging of several gas clouds. In any case, the timescale for both processes should be shorter than 0.5 Gyr, so that the ellipticals form very rapidly. The rapid gas assembly triggers an intense and rapid star-formation process that lasts until a galactic wind, powered by the thermal energy injected by stellar winds and SNe (Ia, II) explosions, occurs. At that time, the thermal energy is equal or larger than the binding energy of gas, and all the residual gas is assumed to be lost. After the wind, the star formation stops and the galaxies evolve passively. The evolution of the global metallicity as well as of 21 single chemical elements are studied in detail. Those elements are produced by single low and intermediate mass stars (AGB stars), SNe Ia, single massive stars (SNe II) and Type Ia SNe(white dwarfs in binary systems). The yields used in this paper are as follows: 1) For single low and intermediate mass stars ($0.8 \leq M/M_{\odot} \leq 8$) we make use of the yields by van den Hoek & Groenewegen (1997) as a function of metallicity; 2) For SNe Ia and SNe II we adopt the empirical yields by François et al. (2004). These yields are a revised version of the Woosley & Weaver (1995) (for SNe II) and Iwamoto et al. (1999) (for SNe Ia) calculations adjusted to best fit the chemical abundances in the Milky Way. We consider that the dust producers are AGB stars, SNe Ia and SNe II. We also take in to account the dust accretion and dust destruction processes in the ISM. Only the main refractory elements, C, O, Mg, Si, S, Ca, Fe, are depleted into dust, and we assume that stars can produce two different types of grains: i) silicate dust, composed of O, Mg, Si, S, Ca and Fe; and ii) carbon dust (graphite in the GRASIL language), composed of C. Since there is no AGN signature in MIPS-LBGs rest-frame UV spectra as well as in their SED, we do not include QSO dust in this paper.

2.2. The spectro-photometric model

Using the SFH, chemical and dust evolution of a galaxy extracted from the chemical evolution model (e.g. as shown in Fig1 and Fig. 2(a)-2(c)), we synthesize the SED of that galaxy with the spectro-photometric code GRASIL (Silva et al. 1998). Briefly, emissions from stellar populations are calculated by evolutionary population synthesis technique (Bressan et al. 1994) using the chemical evolution model and the Padova simple stellar population model (Bertelli et al. 1994). Younger stellar generations are more affected by dust obscuration in their birth place (molecular

Table 1: Chemical model parameters and results.

model name	M_{lum} (M_{\odot})	R_{eff} (kpc)	ν (Gyr^{-1})	τ (Gyr)	t_{gw} (Gyr)	SW yields	SNe Ia and SN II yields	dust elements
M310	3×10^{10}	2	3	0.5	0.8	V&G	François	C, Si, Fe, Mg, O, (S, Ca)
M11	10^{11}	3	10	0.4	0.7	V&G	François	C, Si, Fe, Mg, O, (S, Ca)
M511	5×10^{11}	6	15	0.3	0.7	V&G	François	C, Si, Fe, Mg, O, (S, Ca)

M_{lum} : the total mass of the galaxy at galactic wind time t_{gw} .

R_{eff} : the effective radius of the galaxy.

ν : the star formation efficiency.

τ : the infall time scale.

t_{gw} : the galactic wind time. It is determined only by M_{lum} (and hence ν and τ). Note that it is shorter than in Pipino et al. (2011). This is because the t_{gw} refers to the central region of the galaxy in Pipino et al. (2011), while it refers to the whole galaxy in this work. This is a feature of the outside-in formation formation scenarios (Pipino & Matteucci 2004).

Single low and intermediate mass stars yields (SW yields) are from van den Hoek & Groenewegen (1997) (V&G).

SNe Ia and SNe II yields are from François et al. (2004).

C, Si, Fe, Mg, O are the dust elements adopted in GRASIL, while S, Ca are also the dust elements in chemical models.

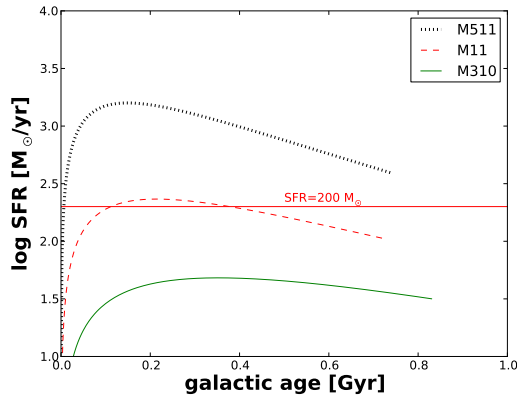
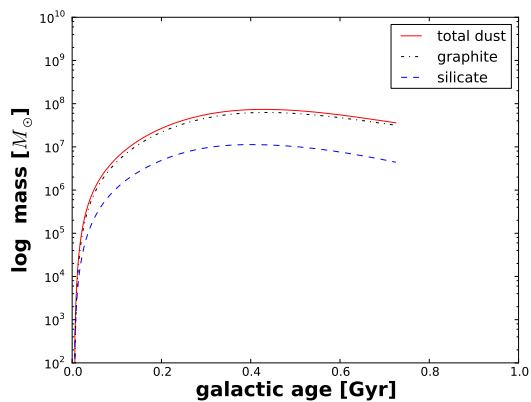
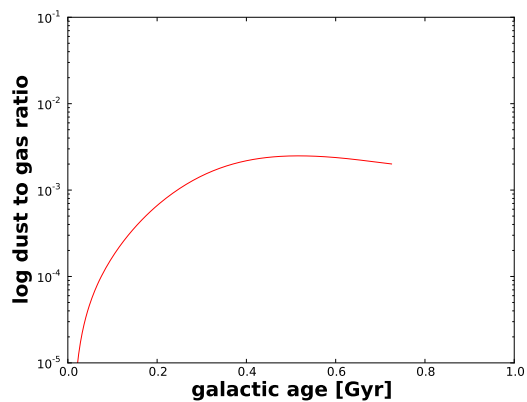


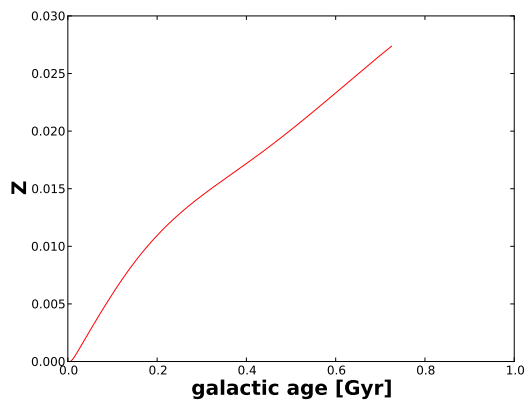
Fig. 1.— The SFR versus time in different mass galaxies. M511, M11 and M310 represent 5×10^{11} , 10^{11} and $3 \times 10^{10} M_{\odot}$ galaxies, respectively. The red horizontal line corresponds to a $SFR=200 M_{\odot}/yr$, which is the estimated value for the average MIPS-LBGs.



(a) Total (red solid line), graphite (black dot line) and silicate (blue dashed line) dust mass of $10^{11} M_{\odot}$ galaxy as a function of galactic age.



(b) Dust to gas ratio of $10^{11} M_{\odot}$ galaxy as a function of galactic age.



(c) Metallicity of $10^{11} M_{\odot}$ galaxy as a function of galactic age.

Fig. 2.— Output of the chemical evolution models adopted by GRASIL. Values in the star forming phase are shown, since we only focus on this phase.

clouds) than older ones in diffuse ISM. The effect of the age selective extinction of stellar populations, for the first time, was modeled by a parametric approach adopting the parameter t_{esc} in GRASIL (Silva et al. 1998). This is described in GRASIL assuming that the fraction of starlight radiated inside the clouds by stars is a function of the star age. In practice, if t_{esc} is the timescale for the process, 100% of the stars younger than t_{esc} are considered to radiate inside the MCs, and this percentage goes linearly to 0% in $2t_{esc}$. The dust composition in GRASIL consists of graphite and silicate grains, and Polycyclic Aromatic Hydrocarbons (PAH) molecules, with a distribution of grain sizes for each composition. The optical properties of silicate and graphite grains are taken from Laor & Draine (1993). The optical properties of PAH molecules are taken from Draine & Li (2007). Dust abundance and dust composition relative abundances are obtained directly from the chemical evolution model. For the molecular clouds a full radiative transfer calculation is performed. The radiative transfer of starlight through dust is computed along the required line of sight yielding the emerging SED (Granato & Danese 1994) based on lambda-iteration numerical method (Efstathiou & Rowan-Robinson 1990; Collison & Fix 1991). However for the diffuse dust, the effects of scattering are only approximated by assuming an effective optical depth related to the true absorption and scattering optical depths by: $\tau_{eff} = [\tau_{abs}(\tau_{abs} + \tau_{sca})]^{1/2}$ and assuming that there is no re-absorption of the radiation emitted by the cirrus.

2.3. The difference between the chemical and spectro-photometric model

The adopted chemical evolution models contain only one gas phase whereas GRASIL takes into account two gas phases: the molecular clouds and diffuse gas. We therefore assume that the chemical and dust-to-gas ratio and dust abundances are the same for those two gas phases. Ca and S are not contained in GRASIL’s dust composition. However, those two elements give a negligible contribution to dust-to-gas ratio. In this paper, we will only consider the following refractory elements: C, Si, Fe, Mg and O. That is, quantities as the total dust mass will be computed neglecting other elements (see 2(b)). The effect caused by the difference between ISM (ISM \equiv gas + dust) metallicity and gas phase metallicity on SED is also negligible. The Salpeter IMF (Salpeter 1955) is adopted in the two models. The baryonic matter (i.e. stars plus gas) is assumed to follow the Jaffe (1983) spatial distribution in the chemical evolution model, while GRASIL adopts the King profile (King 1966) spatial distribution. The spatial distribution, which determines the potential well, only directly affects the galactic wind time in chemical evolution models (see discussion in section 2.1). The geometry effect is not important in the elliptical galaxy SED (e.g. see Silva et al. 1998; Piovan et al. 2006b, for detail). The effects of various parameters on the SED will be discussed in further work in detail. In this paper we only describe the general effects of parameters on deriving physical properties of galaxies.

Table 2: Results from SED fitting for the average MIPS-LBG

Models	MW ^a	MIPS ^b	other works
IR luminosity: $\log(L_{IR}/L_{\odot})$	12.13	12.11	12.21 ^c 12.44 ^d
Stellar mass: M_* (M_{\odot})	8×10^{10}	8×10^{10}	7.9×10^{10} ^e
age (Gyr)	0.5	0.5	1 ^f
SED-derived SFR (M_{\odot}/yr)	200	200	–
IR-derived SFR	233	222	275 ^g
Dust mass: M_d (M_{\odot})	7×10^7	7×10^7	5.5×10^8 ^h
Observational frame 850 μm flux density : $f_{850}(mJy)$	0.16	0.34	1.36 ⁱ
UV Slope: β	-1.6	-2.1	–
Extinction: $E(B - V)$	0.213	0.127	0.1 ^j
Luminosity weighted metallicity: $\langle Z \rangle_{lum}$	0.017	0.017	–
ISM metallicity: Z	0.02	0.02	0.02 ^k
Dust to gas ratio: D_g	0.0025	0.0025	–

a: $10^{11} M_{\odot}$ model (M11) at 0.5 Gyr with WM-like parameters (see Table 3 and 4)

b: $10^{11} M_{\odot}$ model (M11) at 0.5 Gyr with MIPS parameters (see Table 3 and 4)

c, *g* and *i* from Magdis et al. (2010b),

d and *h* from Rigopoulou et al. (2010)

e, *f* and *k* from Magdis et al. (2010a)

j from Magdis's private communication

Table 3: Adopted values of MC in GRASIL

	MW	MIPS
t_{esc} ¹	2	200
f_{mc} ²	0.5	0.5
M_{mc} ³	10^6	10^6
R_{mc} ⁴	40	16

¹ Timescale for the evaporation of MCs, in Myrs.

² Fraction of gas content in the MCs.

³ Total gas mass in each MC, in M_{\odot} .

⁴ Radius of each MC, in pc. The value of R_{mc} in the MW is just to respond to the lower dust-to-gas ratio in the MW than in the star-burst galaxies (see text in Sect. 3.2)

Table 4: Parameters for size distribution of the dust components (Eq. 1 and 2) in the MW and MIPS-LBGs. The MW size distribution is that derived by Silva et al. (1998) to match observations from the MW. The MIPS-LBGs size distributions are calculated in this paper to match SED.

	MW	MIPS LBG
PAH		
X	$3.3 \times 10^{-25} \text{cm}^{2.5}/H$	$5 \times 10^{-25} \text{cm}^{2.5}/H$
Graphite		
a_{min} (Å)	8	...
a_b (Å)	50	8000
a_{max} (Å)	2500	22500
β_1	-3.5	-3.5
β_2	-4.0	...
Silicate		
a_{min} (Å)
a_b (Å)	50	800
a_{max} (Å)	2500	12500
β_1	-3.5	-3.5
β_2

2.4. The fitting approach

In this work, with the help of the SFH, chemical pattern and dust properties from the chemical evolution models (Pipino et al. 2011) and pan-spectral energy distribution data of the stacked MIPS-LBG (Magdis et al. 2010b), we break the SFR-age-metallicity degeneracies for SED modeling. Basically, the flux derived by median stacking analysis represents the average properties of many undetected individual objects. We will not give “ad hoc” parameters but the general properties of the average MIPS-LBG by modelling the stacked SED without taking into account the filter widths in SED fitting. We will adopt an “educated fitting” approach to estimate the physical parameter of the galaxy. This approach is guided by answering these questions: 1) Which parameter dominates the overall-level SED of a galaxy? In other words, from a galaxy SED, which estimated property is most reliable? 2) How do other parameters affect the SED in detail, such as the shape and the peak of some parts of a SED? By means of this approach, we use SFHs suggested by self-consistent chemical evolution models. Moreover, chemical and dust properties, such as metallicity and dust mass, which are the basic ingredients in SED modeling, are given by the same chemical evolution model which gives the SFH. The “fitting” approach is the following: first, since the mass is the most robust parameter in SED fitting (e.g. see Shapley et al. 2005), the total mass of the average MIPS-LBG is estimated by comparing the predicted overall-level of SED with data, and confirmed by further fitting steps. This treatment effectively reduces the computation time, since we do not need to test the MC and dust parameters in GRASIL to estimate the total mass (Step One, see Fig 3). Once the galaxy is selected by total mass estimate, the SFH, chemical and dust evolution history are given by the chemical evolution model with that total mass. Second, the age of the average MIPS-LBG is estimated by comparing the total mass-selected overall-level of SED with data. At this step, the SFR, metallicity, stellar mass, dust mass of the average MIPS-LBG are derived by the SFH adopted in the chemical evolution model (Step Two, see Fig 4). Third, the “best-fitting” dust parameters (shown in Table 3 and 4) are derived by $\min\text{-}\chi^2$ method based on a grid of testing parameters in GRASIL (see an example of grid models in Fig. 5). At this step, the galactic parameters estimated in previous steps are confirmed by the “best-fitting” SED (Step Three, see Fig 6).

To fit the SED, we have tested in GRASIL many SFHs originating from elliptical models. These models cover a large mass range (from $10^9 M_\odot$ to $10^{12} M_\odot$, see Pipino et al. 2011, for detail). The parameters and results of three examples of tested models with total mass $3 \times 10^{10} M_\odot$ (M310), $10^{11} M_\odot$ (M11) and $5 \times 10^{11} M_\odot$ (M511) are shown in Table 1. SFHs of these three models and the estimated SFR of the average MIPS-LBG are shown in Fig. 1. Dust mass, dust-to-gas ratio and metallicity as a function of galactic age of a typical elliptical of $10^{11} M_\odot$ (the “best-fitting” galaxy, see below) adopted in the GRASIL are shown in Fig. 2(a)-2(c), respectively.

The free parameters in GRASIL, which will be investigated by $\min\text{-}\chi^2$ method in this work,

are the ones related to MCs and dust size distribution. There are four parameters (in Table 3) related to MCs: 1) the time scale t_{esc} of young stars escaping from their birth places (MCs), 2) the fraction of gas content in MCs f_{mc} , 3) the mass of a single MC M_{mc} , 4) the radius of a single MC R_{mc} . Note that, the predicted SED depends on M_{mc} and R_{mc} only through the combination M_{mc}/R_{mc}^2 , which is the true free parameter. The dust size distribution for each dust component is described by the power laws (Eq. 1 and Eq. 2 in Sections 3.2 and 3.3). The parameters of graphite and silicate (in Table 4) are the size lower limit (a_{min}), size upper limit (a_{max}), the connection point of the two power laws (a_b) and the ones related to slopes (β_1 and β_2 in Eq. 2'). The parameter X of PAH size distribution controls the abundance of PAH. The normalization parameters, which control the dust abundance and dust component relative abundances are given by the chemical evolution model (see Sect. 3.2 and 3.3 for detail). Other parameters are the same as in Silva et al. (1998). The standard (Milky Way, MW for short) and our “best-fitting” model parameters adopted in SED modeling are shown in Tables 3 and 4. Effects caused by various IMFs, simple stellar populations and dust optical properties will not be discussed in this paper.

3. Results and discussion

The zero order estimates of the relevant physical quantities (masses, SFRs) are typically derived by global or integral properties, such as overall-level SED and IR luminosity, therefore estimates of those quantities are robust. Other quantities (such as UV slope and the predicted flux at a particular band) depend on the shape of SED, and could be different. Table 2 shows the main fitting properties of the average MIPS-LBG by different models. These models fit the overall-level SED, and predict consistent IR luminosities. Stellar mass and IR-derived SFR in all models are comparable, while other quantities are not necessarily consistent with each other. We will discuss these properties in more detail below.

3.1. Stellar populations

The overall-level rest-frame SED, like the value of the luminosity density or flux density, of a galaxy is dominated by its total galaxy mass. Particularly, the total stellar mass dominate the UV-optical part of the SED and total dust mass dominate the IR part of the SED. In general, stars, such as AGB stars and SNe, are the main sources of dust in a galaxy. A more massive star-forming galaxy contains more stars as well as more dust (e.g. see the case of young elliptical galaxies in Pipino et al. 2011). The more massive star forming galaxy will show higher overall-level rest-frame SED. Since our estimations are based on the UV-radio overall-level SED fitting, our results of the stellar population are derived by a complementary approach comparing to the

normal approach, which is usually based on optical to near-IR SED fitting.

We compare the predicted SEDs of different massive galaxies at different ages (see an example of different massive galaxies at moderate age 0.5 Gyr in Fig. 3. Since short and intense star formation histories are yielded by chemical evolution models, the parameter space of age is not large (age < 0.7Gyr). From Fig. 3 and Fig. 4, we can estimate that the galaxy with total mass $\sim 10^{11} M_{\odot}$ could reproduce the overall-level SED of the average MIPS-LBG. Note that, this mass is the total mass of an elliptical galaxy at the wind time given by the chemical evolution model. In fact, after the wind, no more star are formed and the galaxy evolves passively.

From the modeling point of view, the total stellar mass is dominated by SFH, IMF and the age of stellar populations. Age is the only free parameter of stellar populations when SFH, chemical enrichment history and IMF of a galaxy are fixed. With a given SFH in a chemical model, the SFR is a predictable parameter. By comparing with the value estimated from observational indicators, SFR could constrain the age of a galaxy. UV and IR indicators for SFR (e.g. Kennicutt 1998) have been adopted in the literature for high redshift galaxies. Besides, depending on stellar population synthesis models, the UV-derived SFR depends on the treatment of extinction for deriving the extinction-correct fluxes, and the IR-derived SFR depends on the SED library for converting observed flux (e.g. the flux at $24 \mu m$) to total ($8 - 1000 \mu m$) IR luminosity L_{IR} . This approach has the drawback of assuming the low-redshift template SEDs accurately represent the SED of high-redshift galaxies. For example, the excessive high $850 \mu m$ fluxes predicted by an empirical UV-based relationship and the unreasonable high L_{IR} estimated by MIR flux-IR luminosity correlation in SED templates have caused the problem of non-detection of $z \sim 3$ LBGs in $850 \mu m$ band, reported in Chapman et al. (2000) and Shim et al. (2007) respectively. Additionally, various dust intrinsic properties strongly affect the UV-FIR fluxes (see Fig. 5). Therefore, we need other indicators to estimate the SFR in our SED fitting approach. In GRASIL the non-thermal radio emission, which is not affected by dust intrinsic properties, is proportional to the SN II rate. Since the life of SNe II is very short (< 30 Myr), the SN II rate is proportional to the SFR. So the rest-frame radio flux should be a good estimator of SFR. This is reflected by the fact that both the radio flux and SFR decrease (shown in Fig. 1 and 4) at the age from 0.2 to 0.6 Gyr. For the $10^{11} M_{\odot}$ model, the phase with SFR $\sim 200 M_{\odot}/yr$, corresponding to the age of 0.3 to 0.6 Gyr (see Fig 1), fits the rest-frame radio flux well, and this SFR agrees with the estimation ($\sim 250 M_{\odot}/yr$) of Magdis et al. (2010b). Since we have already selected the $10^{11} M_{\odot}$ model based on overall-level SED, the SFR derived here benefits from the merits of radio-derived and SED-derived approaches, and is remarkably consistent with the IR-derived SFR (see Table 2 and discussion below).

In our approach, the age is estimated by fitting the overall-level SED and the radio flux, namely it is a luminosity weighted age confirmed by “observed” SFR. The SFR and total mass suggest that the ages of MIPS-LBGs should be $\sim 0.3 - 0.6$ Gyr (see Fig. 4), and younger than

0.7 Gyr since the LBGs are star-forming galaxies. Note that, the estimated $\text{SFR} = 200M_{\odot}/\text{yr}$ is a typical SFR in the age range of 0.3 to 0.6 Gyr. The SFR is $221M_{\odot}/\text{yr}$ and $140M_{\odot}/\text{yr}$ at 0.3 and 0.6 Gyr for the $10^{11}M_{\odot}$ model, respectively. The total stellar mass is $\sim 6 \times 10^{10}M_{\odot}$ and $\sim 1 \times 10^{11}M_{\odot}$ at 0.3 and 0.6 Gyr for the $10^{11}M_{\odot}$ model, respectively. We adopt 0.5 Gyr for the next fitting step. This age corresponds to $\text{SFR} \sim 185M_{\odot}/\text{yr}$ and total stellar mass $\sim 8 \times 10^{10}M_{\odot}$, which agrees with the value ($\sim 7.9 \times 10^{10}M_{\odot}$) of Magdis et al. (2010b). Our age estimate 0.3 – 0.6Gyr is not consistent with the median age $\sim 1\text{Gyr}$ derived by synthesis population model in Magdis et al. (2010a). In particular, our elliptical model does not allow a LBG to be older than 1Gyr. It is however worth reminding, that while the star formation history predicted in chemical evolution models is modulated by the gas infall and self-consistently quenched due to SN-driven wind, this does not happen in the template star formation histories adopted in standard SED fitting, and this might cause the disagreement in the age estimate.

3.2. Dust properties

As molecular clouds (MCs) are the birth place of stars, studying properties of MCs at high redshift is important for our understanding of the star forming in galaxies (see review by Riechers 2011). In this paper, we assume that all the MCs have the same mass M_{mc} and spherical radius R_{mc} . MCs make much more contributions in extinction than diffuse ISM in a star-burst galaxy with the fractionary gas content in the MCs $f_{MC} \geq 0.5$. The parameter t_{esc} shown in Table 3 controls how long the young stars remain in their birth clouds and roughly controls the fraction of extinguished stellar light, therefore it controls the total level of rest-frame UV-optical SED and the slope of the rest-frame UV-optical SED. The optical depth of dust in a MC is determined by the dust-to-gas ratio δ times M_{mc}/R_{mc}^2 . This parameter moderately controls the total level of rest-frame UV-optical SED and also affects the slope of rest-frame UV-optical SED. The “best-fitting” parameters of MCs for the average MIPS-LBGs are shown in Table 4. The larger value of the t_{esc} and the smaller value of the R_{mc} compared with the MW ones⁷ imply that the MCs in the average MIPS-LBG are likely to be in more dense dusty environments. The same trend is found in local and high redshift starburst galaxies (Silva et al. 1998; Schurer et al. 2009; Swinbank et al. 2011). Yan et al. (2010) suggested that the average molecular gas mass of $24\mu\text{m}$ detected ultra-luminous infrared galaxies (ULIRGs, $L_{IR} > 10^{12}L_{\odot}$) at $z = 1.6 - 2.5$ is $1.7 \times 10^{10}M_{\odot}$ by observed CO J=2 \rightarrow 1 or J=3 \rightarrow 2

⁷The values of MC parameters of the MW are the same as in spiral models in Schurer et al. (2009), except for R_{mc} . The dust-to-gas ratio is given by the chemical evolution models and not modified by GRASIL in this work. Since we do not use the spiral SED models, we adopt a larger value of R_{MC} for the MW responding to the effect of lower optical depth caused by lower dust-to-gas in the MW than in star-burst galaxies. In any case, the t_{esc} is the dominant parameter.

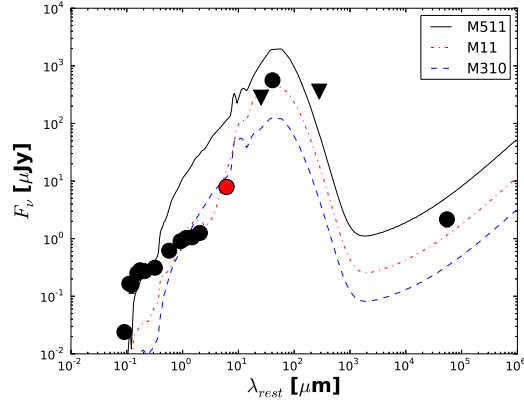


Fig. 3.— Rest-frame SEDs of different models. M511, M11 and M310 represent 5×10^{11} , 10^{11} and $3 \times 10^{10} M_\odot$ galaxies with star burst SFH at 0.5 Gyr with the MW dust parameters shown in Table 3 and Table 4, respectively. Data are from Magdis et al. (2010b): for the SED we use the median UGR+BViJK+IRAC+MIPS24 photometry of MIPS-LBGs, and the values (or upper limits) derived from stacking $100 \mu\text{m}$, $160 \mu\text{m}$ AzTEC and radio, divided by $1 + z$. Downward triangles are up-limits. The MIPS data is indicated with a red point. At the first fitting step, the $10^{11} M_\odot$ model is empirically selected for next fitting step.

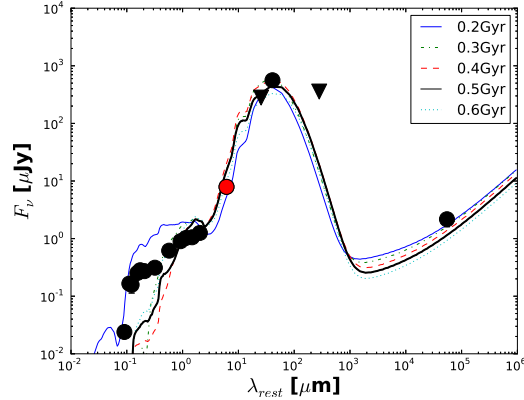


Fig. 4.— Rest-frame SED of a $10^{11} M_\odot$ galaxy at different ages with the MW dust parameters as in Table 3 and Table 4. The parameter space of age is < 0.7 Gyr. The model with age 0.3 – 0.6 Gyr could fit the overall-level SED. At the second fitting step, the $10^{11} M_\odot$ galaxy at 0.5 Gyr is the model adopted for further fitting step. This model predicts comparable SFR and stellar mass with other people’s work (see text for detail). MIPS-LBGs data are from Magdis et al. (2010b) as described in Fig 3.

emission. Our total gas mass M_g in $10^{11} M_\odot$ galaxy at 0.5 Gyr is $1.6 \times 10^{10} M_\odot$. With fractionary gas content in the MCs $f_{MC} = 0.5$, the total mass in molecular clouds in our “best-fitting” model is $0.8 \times 10^{10} M_\odot$. However, the lack of emission lines makes it difficult to break the degeneracy of the MC conditions and dust size distribution.

Once the emission from stellar populations is set, the peak in the emission in far-IR (FIR) is dominated by the total cold dust mass. The total dust mass M_d is $\sim 7 \times 10^7 M_\odot$ in “best-fitting” $10^{11} M_\odot$ model at 0.5 Gyr. It is about a factor of eight less than the value ($M_d = 5.5 \pm 1.6 \times 10^8 M_\odot$ in Rigopoulou et al. 2010) based on single temperature grey-body fitting (Hildebrand 1983). This may partly be caused by three facts: 1) the uncertainty in the galaxy mass estimate, therefore the dust mass value in this work. Since the dust mass is a consequence of the galaxy evolution in our chemical models, the estimated total galactic mass affects the total dust mass. For example, a $2 \times 10^{11} M_\odot$ galaxy⁸ at 0.5 Gyr produces a dust mass $M_d \sim 2 \times 10^8 M_\odot$. 2) The well known degeneracy of dust temperature T_d and slope β_d in single temperature grey-body fitting (Blain et al. 2003). A higher β_d will result in lower dust temperature derived from single temperature grey-body fitting (Sajina et al. 2006), therefore a higher dust mass will be estimated. 3) The uncertainty of single temperature grey-body fitting parameter, such as the rest-frame dust mass absorption coefficient κ (e.g. a factor ~ 7 at $800 \mu\text{m}$ estimated by Hughes et al. 1997). Note that, the single temperature grey-body fitting could predict a higher IR flux than the value by full SED fitting. An example is shown in Magdis et al. (2010b). The value of the far-IR emission peak predicted by the single temperature grey-body fitting shown in their Fig. 4 is larger than 1 mJy , while the peak value shown in their Fig. 2 is smaller than 1 mJy predicted by SED fitting.

Prominent PAH features are observed in MIPS-LBGs (Huang et al. 2007). In star-burst galaxies, the mid-IR (MIR) flux is contributed by small hot dust and PAH (see e.g. Laurent et al. 2000, and references therein). The abundance of PAHs of our model is calculated from the chemical composition of the dust as predicted by the chemical evolution model, and their abundance is proportional to the total abundance of carbon molecules in the dusty component of the ISM. The PAH size distribution adopted in GRASIL is :

$$\frac{dn}{da} = Xa^{-3.5} \text{cm}^{-1}. \quad (1)$$

PAH is needed in the “best-fitting” model to fit the average MIPS-LBG MIR flux (see Fig.6). However, we cannot put more constraints on the PAH without emission lines. The “best-fitting” model gives $X = 5 \times 10^{-25} \text{cm}^{2.5}/H$ ($X = 3.3 \times 10^{-25} \text{cm}^{2.5}/H$ in Silva et al. (1998)).

⁸deviation of estimated total galaxy mass from the “best-fitting” value within a factor of two is normal and acceptable in all SED fitting work.

3.3. Dust intrinsic properties

For many years, many efforts have been spent on investigating the dust size distribution through three approaches: i) theoretical approach (e.g. Birnstiel et al. 2011), ii) fitting extinction curve approach (e.g. Mathis et al. 1977; Weingartner & Draine 2001; Clayton et al. 2003; Zubko et al. 2004) and iii) by means of the SED approach (e.g. Carciofi et al. 2004; Takeuchi & Ishii 2004; Piovan et al. 2006a). However, the nature of dust size distribution is still not clear, especially for in high redshift objects.

The position of the peak in FIR is mainly affected by the total dust mass, dust component relative abundances and dust size distribution, but not by the stellar populations (see Fig.3 and Slater et al. 2011). With the help of chemical evolution models, which predict the total dust mass and dust component relative abundance, we can study the dust size distribution in a more reliable way. The graphite and silicate grains dust size distribution strongly affect the slope of the rest-frame UV-optical SED. For the sake of simplicity, a simple power law dust size distribution form is adopted in this paper. The dust size distribution for the i (graphite or silicate) composition follows a broken power law defined with a threshold a_b :

$$\frac{dn_i}{da} = \begin{cases} A_i n_H a^{\beta_1}, & \text{if } a_b < a < a_{max}, \\ A_i n_H a_b^{\beta_1 - \beta_2} a^{\beta_2}, & \text{if } a_{min} < a < a_b. \end{cases} \quad (2)$$

$$(2')$$

For the sake of simplicity, dust in MIPS-LBGs only use Eq. 2 (see Table 4). The dust mass m_i and dust-to-gas ratio δ are provided by the chemical evolution model:

$$m_i = \int_{a_{min}}^{a_{max}} \frac{4\pi a^3 \rho_i}{3n_H} \frac{dn_i}{da} da, \quad (3)$$

$$\delta = \frac{\sum_i m_i}{m_H}, \quad (4)$$

where n_H , m_H and ρ_i are the gas number density, gas mass and grain mass density, respectively. The normalized parameter A_i is calculated by Eq. 2, 3, 4. Comparing with the dust size distribution in the MW (see Table 4), a larger amount of dust with larger size is needed to fit the slope of rest-frame UV-optical SED (see Fig. 5 and Fig. 6). With the theoretical indication of a few μm size (e.g. Tanaka et al. 2005; Birnstiel et al. 2009) and observational suggestion of up to cm-sizes (e.g. Rodmann et al. 2006; Ricci et al. 2010), our estimation of maximum dust size $a_{max}=2.2 \mu\text{m}$ is acceptable.

With indications from both the peak and the position of FIR and the slope of rest-frame UV-optical SED, we suggest that the dust size distribution of the average MIPS-LBG is top-heavy (flatter) comparing with that in the MW. The reliability of this trend for all high redshift LBGs needs more data to provide more reliable constraints for the models in the future.

3.4. The impact of the adopted SFH

The adopted SFH is the main input ingredient which produces different predictions on detailed physical processes by means of population synthesis modeling. By the standard SED fitting, we cannot rule out other SFHs than the ones adopted. For example, Fig. 7. shows two models adopting a self-consistent star formation history (SFH of M11 case in Fig.1, SSF for short) and a constant star formation history (CSF). These two models can produce similar overall-level SEDs with fine-tuning of the ages corresponding to comparable stellar masses. In this paper, to improve the reliability of the adopted SFH for the $z \sim 3$ MIPS-LBGs, we adopted chemical model constrained SFHs, which have been successfully reproduced the chemical data of several $z \sim 3$ LBGs.

The stellar mass derived by Elliptical-type star-burst SFH in this work is consistent with other works, although we used a different SED model and fitting approach to fit the SED. Again, this is because the stellar mass is a more robust parameter than other parameters, such as age, which have been found in other SED fitting works (e.g. Papovich et al. 2001; Shapley et al. 2005; Magdis et al. 2010a). Recently, Lo Faro et al. (2013) found discrepancies between their results and those based on optical-only SED fitting for the same objects. By fitting observed SEDs with their physical model, they found higher stellar masses (by $\Delta M_* \sim 1.4$ and 2.5 dex) resulting from higher extinction (the average total extinction in the rest-frame V-band $A_V \sim 0.81$ and 1.14) for $z \sim 1$ and $z \sim 2$ dusty normal star-forming (e.g. $\text{SFR} \leq 10 M_\odot \text{yr}^{-1}$) galaxies, respectively. With only one average $z \sim 3$ dusty star-forming galaxies in our paper, it is hard to test whether there is also a same systematic discrepancy, and the discrepancy is mainly caused by extinction for $z \sim 3$ dusty star-burst (e.g. $\text{SFR} > 100 M_\odot \text{yr}^{-1}$) galaxies or not. We would like point out that the dusty star-forming galaxies at different redshifts are not necessarily linked from an evolutionary point of view, therefore the types of SFH and the evolution phases in which galaxies are observed might be different. Therefore, one might get comparable stellar mass by the full SED fitting and optical-only SED fitting with different ages and extinction values (laws). For example, by playing with dust parameters in the CSF case shown in Fig. 7, we would expect to fit the optical-only SED at 2 Gyr estimating a stellar mass $\sim 9 \times 10^{10}$ which is comparable with the stellar mass $\sim 8 \times 10^{10}$ at 0.5 Gyr in the “best-fitting” model by full-SED fitting.

Unlike the stellar mass, our estimated age (~ 0.5 Gyr) is younger than other works (~ 1 Gyr). Our intense star-burst SFH allows the galaxy to form enough stars and dust to produce the overall-level SED at that age. Dust makes the key link between the UV-optical SED and IR SED. In the standard SED fitting approach, dust mass cannot be derived, therefore it does not depend on the adopted SFH. In our approach, dust mass is a consequence of galaxy and dust evolution in the chemical models and depends on the SFH. By assuming reasonable detailed dust properties, the dust in our model interacting with stellar light, reproduces the SED of the average MIPS-LBG. The

value of the dust mass in our work is about a factor of eight less than the value in Rigopoulou et al. (2010) based on single temperature grey-body fitting (see discussion in Sect. 3.2). Note that, our predictions on dust environment and dust intrinsic properties correspond to “best-fitting” SED of the average MIPS-LBG, and further work/data about these MIPS-LBGs are needed to confirm this result.

Clearly, the high SFR shown in the LBGs could be triggered by galaxy-merger, which means completely different SFH and physical processes. This scenario of galaxy evolution is not considered in this work. We hope that more data in the future, such as the galaxy morphology and chemical abundances, will reveal the nature of all LBGs.

Having discussed the limitations in our approach, we will compare our “best-fitting” model for the average MIPS-LBG with other objects which show similar observed features in some aspects.

3.5. Comparison with lower mass $z \sim 3$ LBGs

The gravitational lensed LBG cB58 is the best-studied typical LBG. This object is at $z \sim 2.73$ and has a luminous mass $\sim 10^{10} M_{\odot}$, a SFR $\sim 40 M_{\odot} \text{yr}^{-1}$ (Pettini et al. 2002) and an effective radius of $r_L \sim 2$ kpc (Seitz et al. 1998), for a $\Omega_m = 0.3, \Omega_{\Lambda} = 0.7, h = 0.70$ cosmology. The average MIPS-LBG, with total mass $\sim 10^{11} M_{\odot}$ estimated in this work, is more massive than cB58 (cB58 is $10^{10} - 3 \times 10^{10} M_{\odot}$ in Pipino et al. 2011). The model suggests a SFR $\sim 200 M_{\odot} / \text{yr}$ for the average MIPS-LBG, which is higher than that of cB58. The metallicity of MIPS-LBGs ($\sim Z_{\odot}$) is higher than cB58 ($\sim 0.25 Z_{\odot}$). These differences imply that MIPS-LBGs and cB58 are at the opposite ends of the observed mass-SFR (Magdis et al. 2010a) and mass-metallicity (Maiolino et al., 2008) relations at $z \sim 3$.

The shape of a galaxy SED depends on many physical processes as we have shown above. We compare the average MIPS-LBG in this work with other $24\mu\text{m}$ MIPS detected $z \sim 3$ LBGs (Rigopoulou et al. 2006; Shim et al. 2007) in Fig. 8 by plotting the estimated extinction $E(V - B)$ versus observed $24\mu\text{m}$ flux density f_{24} . As shown in Fig. 8, the observed frame f_{24} does not correlate with the $E(B - V)$ for these samples. One could not derive reliable IR properties only based on fitted parameters, which describe UV-optical properties. Therefore, we suggest that self-consistent SED models are needed when deriving detail properties of galaxies from their UV-radio multi-band data

3.6. Comparison with submillimetre galaxies (SMGs)

The MIPS-LBGs with IR luminosity of $L_{IR} = 1.3 \times 10^{12} L_{\odot}$ is in the class of ultra-luminous infrared galaxies (ULIRGs, $L_{IR} > 10^{12} L_{\odot}$). Since MIPS-LBGs could be the most massive, dusty, star-forming and young ellipticals as discussed in the above section, we suggest that these ellipticals contribute a significant population for ULIRGs at redshift $z \sim 3$. The non detection of infrared luminous LBGs in submm band is a puzzle, given their large L_{IR} and high UV-derived SFR, as well as substantial dust component (see detail in Chapman et al. (2000) and Shim et al. (2007)). There are only two detections of FIR counterparts of MIPS-LBGs reported in the literature (Chapman et al. 2000; Chapman & Casey 2009). The higher dust temperature, different dust spatial distribution and lower SFR in LBGs than in SMGs have been suggested to explain this challenge (e.g. Chapman et al. 2000; Rigopoulou et al. 2006; Magdis et al. 2010b). Based on our “best-fitting” model, our prediction of observational frame flux density of MIPS-LBGs at $850\mu\text{m}$ is 0.3mJy , which is under the confusion/detection limit of current submillimetre (submm) surveys ($f_{850} = 1\text{mJy}$ and $f_{850} = 2\text{mJy}$). Note that, our $850\mu\text{m}$ flux density $f_{850} = 0.3\text{mJy}$ is lower than $f_{850} = 1.36\text{mJy}$ (Magdis et al. 2010b) predicted by the “best-fitting” SED from templates (Chary & Elbaz 2001), while the IR luminosity of our model and other models are comparable (see Table 2). This reflects the fact that the predicted flux could be quite different at a particular wavelength, although a few observed fluxes or the overall-level SED (e.g. the IR luminosity) could be comparable, since the shape of SEDs could be quite different. The detailed SED of a galaxy depends on all physical processes in our model. Besides the explanations mentioned in the literature, we suggest the different galaxy morphology, dust environment and dust intrinsic properties could also cause the non detection of LBGs in submm blank survey. However, it is hard to make a conclusion about the link between LBGs and SMGs before more data, such as a large population with detailed SEDs and chemical abundances, are available.

The dust temperatures are merely those corresponding to the best-fitting single temperature grey-body model, and are not the actual dust temperature. We use the rest-frame 100-to-850 μm flux density ratio versus 60-to-850 μm flux density ratio, f_{100}/f_{850} vs f_{60}/f_{850} , as a proxy to FIR properties of galaxies. Our predictions of M310, M11, M511 models from 0.1 Gyr to 0.7 Gyr are compared with the data of SCUBA local (recession velocity \sim few thousand km s^{-1}) galaxies (Dunne et al. 2000) in Fig. 9. Compared to SCUBA local galaxies, the young high redshift starburst galaxies in our models have much higher f_{60}/f_{850} given the same f_{100}/f_{850} . The more massive galaxies have higher f_{100}/f_{850} and f_{60}/f_{850} . It is clear that the SCUBA local SMGs and young high redshift star-burst galaxies have different FIR properties.

We argue that caution is needed when adopting the local empirical UV-IR relationships and templates for high redshift $z \sim 3$ LBGs to understand the physical processes in detail.

4. Conclusions

In this paper, we modeled the rest frame UV-radio SED of the stacked MIPS-LBG at $z \sim 3$ by a new “fitting” approach. In this self-consistent approach, we derived the average galactic-wide properties of MIPS-LBGs at $z \sim 3$ considering the stacked MIPS-LBG as a proxy of all MIPS-LBGs at $z \sim 3$. Our findings can be summarized as follows:

1. The new “fitting” approach, which combines the chemical evolution model and GRASIL, can reproduce the rest frame UV-radio SED of the stacked MIPS-LBG at $z \sim 3$. This approach suggests that the MIPS-LBGs at $z \sim 3$ are likely young (0.3-0.6 Gyr) massive ($\sim 10^{11} M_{\odot}$) elliptical galaxies with a fast star-burst regime of star formation. Chemical enrichment and dust evolution history are provided by chemical evolution models, calibrated at both low and high redshifts.
2. We estimated that the the average stellar mass of MIPS-LBGs is in the range of $\sim 6 \times 10^{10} M_{\odot}$ to $\sim 1 \times 10^{11} M_{\odot}$. The “best-fitting” stellar mass and SFR of the stacked MIPS-LBG are $8 \times 10^{10} M_{\odot}$ and $200 M_{\odot}/yr$, respectively. The stellar mass is in agreement with estimates done in other works and based on UV-optical SED fitting. This confirms that the derived stellar mass is robust in SED fitting.
3. The “best-fitting” model of the stacked MIPS-LBG is the 0.5 Gyr $10^{11} M_{\odot}$ elliptical galaxy, which has dust mass of $M_d = 7 \times 10^7 M_{\odot}$ and gas mass of $M_g = 1.6 \times 10^{10} M_{\odot}$. Our “best-fitting” dust mass of the stacked MIPS-LBG is about a factor of eight less than the value based on single temperature grey-body fitting ($M_d = 5.5 \pm 1.6 \times 10^8 M_{\odot}$ in Rigopoulou et al. 2010).
4. The parameters of molecular clouds and dust of the Milky Way cannot fit the stacked MIPS-LBG SED. Our “best-fitting” parameters reflect that: i) MCs of the stacked MIPS-LBG are more dense dusty environments than in the Milky Way; ii) the dust size distributions in stacked MIPS-LBG may be flatter than in the Milky Way; iii) both small and big size dust are needed to reproduce the stacked MIPS-LBG SED; iv) non-negligible PAH also make an important contribution to MIR flux. More observational data, such as chemical abundances and emission lines, are needed to make a more realistic prediction of the properties of all MIPS-LBGs, especially for dust intrinsic properties.
5. We suggest that high redshifts star-forming ellipticals make a significant contribution to the population of ULIRGs. The dust properties and morphology of high redshift star-burst galaxies could be different from local star-burst galaxies. We argue that self-consistent SED models are needed to investigate the detailed properties of high redshift LBGs .

Acknowledgments

We thank the anonymous referee for valuable comments and useful suggestions which improved this work very much. We thanks G.E. Magids for providing the stacked MIPS-LBGs data and T. Bschorr for useful comments. X.L. Fan also thanks L. Silva and G. Granato for proving GRASIL and for many useful discussions. F. Matteucci acknowledges financial support from PRIN MIUR2010-2011, Project "The Chemical and Dynamical Evolution of the Milky Way and Local Group Galaxies", prot. N.2010LY5N2T. X.L. Fan acknowledges financial support from NSFC (Grant No 11243006).

REFERENCES

- Bertelli, G., Bressan, A., Chiosi, C., Fagotto, F., & Nasi, E. 1994, *A&AS*, 106, 275
- Birnstiel, T., Dullemond, C. P., & Brauer, F. 2009, *A&A*, 503, L5
- Birnstiel, T., Ormel, C. W., & Dullemond, C. P. 2011, *A&A*, 525, A11+
- Blain, A. W., Barnard, V. E., & Chapman, S. C. 2003, *MNRAS*, 338, 733
- Bressan, A., Chiosi, C., & Fagotto, F. 1994, *ApJS*, 94, 63
- Burgarella, D., Le Floch, E., Takeuchi, T. T., Huang, J. S., Buat, V., Rieke, G. H., & Tyler, K. D. 2007, *MNRAS*, 380, 986
- Calura, F., Pipino, A., Chiappini, C., Matteucci, F., & Maiolino, R. 2009, *A&A*, 504, 373
- Calura, F., Pipino, A., & Matteucci, F. 2008, *A&A*, 479, 669
- Carciofi, A. C., Bjorkman, J. E., & Magalhães, A. M. 2004, *ApJ*, 604, 238
- Clayton, G. C., Wolff, M. J., Sofia, U. J., Gordon, K. D., & Misselt, K. A. 2003, *ApJ*, 588, 871
- Collison, A. J., & Fix, J. D. 1991, *ApJ*, 368, 545
- Daddi, E., et al. 2007, *ApJ*, 670, 156
- Davé, R., Gardner, J., Hernquist, L., Katz, N., & Weinberg, D. 2000, in *Astronomical Society of the Pacific Conference Series*, Vol. 200, *Clustering at High Redshift*, ed. A. Mazure, O. Le Fèvre, & V. Le Brun, 173–+
- Draine, B. T., & Li, A. 2007, *ApJ*, 657, 810

- Dunne, L., Eales, S., Edmunds, M., Ivison, R., Alexander, P., & Clements, D. L. 2000, MNRAS, 315, 115
- Eales, S. A., & Edmunds, M. G. 1996, MNRAS, 280, 1167
- Efstathiou, A., & Rowan-Robinson, M. 1990, MNRAS, 245, 275
- Erb, D. K., Shapley, A. E., Pettini, M., Steidel, C. C., Reddy, N. A., & Adelberger, K. L. 2006a, ApJ, 644, 813
- Erb, D. K., Steidel, C. C., Shapley, A. E., Pettini, M., Reddy, N. A., & Adelberger, K. L. 2006b, ApJ, 646, 107
- François, P., Matteucci, F., Cayrel, R., Spite, M., Spite, F., & Chiappini, C. 2004, A&A, 421, 613
- Friaca, A. C. S., & Terlevich, R. J. 1999, MNRAS, 305, 90
- Gawiser, E. 2009, NewAR, 53, 50
- Genzel, R., et al. 2010, MNRAS, 407, 2091
- . 2011, ApJ, 733, 101
- Gnerucci, A., et al. 2011, A&A, 528, A88
- Granato, G. L., & Danese, L. 1994, MNRAS, 268, 235
- Hainline, K. N., Shapley, A. E., Kornei, K. A., Pettini, M., Buckley-Geer, E., Allam, S. S., & Tucker, D. L. 2009, ApJ, 701, 52
- Hildebrand, R. H. 1983, QJRAS, 24, 267
- Hopkins, A. M., & Beacom, J. F. 2006, ApJ, 651, 142
- Huang, J., et al. 2007, ApJ, 660, L69
- Hughes, D. H., Dunlop, J. S., & Rawlings, S. 1997, MNRAS, 289, 766
- Iwamoto, K., Brachwitz, F., Nomoto, K., Kishimoto, N., Umeda, H., Hix, W. R., & Thielemann, F. 1999, ApJS, 125, 439
- Jaffe, W. 1983, MNRAS, 202, 995
- King, I. R. 1966, AJ, 71, 64
- Laor, A., & Draine, B. T. 1993, ApJ, 402, 441

- Laurent, O., Mirabel, I. F., Charmandaris, V., Gallais, P., Madden, S. C., Sauvage, M., Vigroux, L., & Cesarsky, C. 2000, *A&A*, 359, 887
- Law, D. R., Steidel, C. C., Shapley, A. E., Nagy, S. R., Reddy, N. A., & Erb, D. K. 2012, *ArXiv e-prints*, 1206.6889
- Magdis, G. E., Rigopoulou, D., Huang, J., & Fazio, G. G. 2010a, *MNRAS*, 401, 1521
- Magdis, G. E., Rigopoulou, D., Huang, J., Fazio, G. G., Willner, S. P., & Ashby, M. L. N. 2008, *MNRAS*, 386, 11
- Magdis, G. E., et al. 2010b, *ApJ*, 720, L185
- . 2011, *A&A*, 534, A15
- Maiolino, R., et al. 2008, *A&A*, 488, 463
- Mannucci, F., et al. 2009, *MNRAS*, 398, 1915
- Mathis, J. S., Ruml, W., & Nordsieck, K. H. 1977, *ApJ*, 217, 425
- Matteucci, F., & Pipino, A. 2002, *ApJ*, 569, L69
- Papovich, C., Dickinson, M., & Ferguson, H. C. 2001, *ApJ*, 559, 620
- Pentericci, L., Grazian, A., Scarlata, C., Fontana, A., Castellano, M., Giallongo, E., & Vanzella, E. 2010, *A&A*, 514, A64+
- Pettini, M., Rix, S. A., Steidel, C. C., Adelberger, K. L., Hunt, M. P., & Shapley, A. E. 2002, *ApJ*, 569, 742
- Pettini, M., Steidel, C. C., Adelberger, K. L., Dickinson, M., & Giavalisco, M. 2000, *ApJ*, 528, 96
- Piovan, L., Tantalò, R., & Chiosi, C. 2006a, *MNRAS*, 366, 923
- . 2006b, *MNRAS*, 370, 1454
- Pipino, A., Fan, X. L., Matteucci, F., Calura, F., Silva, L., Granato, G., & Maiolino, R. 2011, *A&A*, 525, A61+
- Pipino, A., & Matteucci, F. 2004, *MNRAS*, 347, 968
- Reddy, N. A., Erb, D. K., Pettini, M., Steidel, C. C., & Shapley, A. E. 2010, *ApJ*, 712, 1070
- Reddy, N. A., Steidel, C. C., Pettini, M., Adelberger, K. L., Shapley, A. E., Erb, D. K., & Dickinson, M. 2008, *ApJS*, 175, 48

- Ricci, L., Testi, L., Natta, A., Neri, R., Cabrit, S., & Herczeg, G. J. 2010, *A&A*, 512, A15+
- Riechers, D. A. 2011, ArXiv e-prints, 1103.3897
- Rigopoulou, D., et al. 2010, *MNRAS*, L154+
- Rodmann, J., Henning, T., Chandler, C. J., Mundy, L. G., & Wilner, D. J. 2006, *A&A*, 446, 211
- Sajina, A., Scott, D., Dennefeld, M., Dole, H., Lacy, M., & Lagache, G. 2006, *MNRAS*, 369, 939
- Salpeter, E. E. 1955, *ApJ*, 121, 161
- Sawicki, M., & Yee, H. K. C. 1998, *AJ*, 115, 1329
- Schurer, A., Calura, F., Silva, L., Pipino, A., Granato, G. L., Matteucci, F., & Maiolino, R. 2009, *MNRAS*, 394, 2001
- Shapley, A. E. 2011, *ARA&A*, 49, 525
- Shapley, A. E. 2011, *ARA&A*, 49, 525
- Shapley, A. E., Steidel, C. C., Erb, D. K., Reddy, N. A., Adelberger, K. L., Pettini, M., Barmby, P., & Huang, J. 2005, *ApJ*, 626, 698
- Silva, L., Granato, G. L., Bressan, A., & Danese, L. 1998, *ApJ*, 509, 103
- Slater, C. T., et al. 2011, ArXiv e-prints, 1103.2170
- Steidel, C. C. and Hamilton, D. 1993, *AJ*, 105, 2017S
- Takeuchi, T. T., & Ishii, T. T. 2004, *A&A*, 426, 425
- Steidel, C. C., Adelberger, K. L., Shapley, A. E., Pettini, M., Dickinson, M., & Giavalisco, M. 2003, *ApJ*, 592, 728
- Steidel, C. C., Shapley, A. E., Pettini, M., Adelberger, K. L., Erb, D. K., Reddy, N. A., & Hunt, M. P. 2004, *ApJ*, 604, 534
- Swinbank, M., et al. 2011, ArXiv e-prints, 1110.2780
- Takeuchi, T. T., & Ishii, T. T. 2004, *A&A*, 426, 425
- Tanaka, H., Himeno, Y., & Ida, S. 2005, *ApJ*, 625, 414
- Thomas, D., Maraston, C., Bender, R., & Mendes de Oliveira, C. 2005, *ApJ*, 621, 673

- van den Hoek, L. B., & Groenewegen, M. A. T. 1997, *A&AS*, 123, 305
- Vanzella, E., et al. 2009, *ApJ*, 695, 1163
- Vijh, U. P., Witt, A. N., & Gordon, K. D. 2003, *ApJ*, 587, 533
- Walcher, J., Groves, B., Budavári, T., & Dale, D. 2011, *Ap&SS*, 331, 1
- Weingartner, J. C., & Draine, B. T. 2001, *ApJ*, 548, 296
- Woosley, S. E., & Weaver, T. A. 1995, *ApJS*, 101, 181
- Yan, L., et al. 2010, *ApJ*, 714, 100
- Zubko, V., Dwek, E., & Arendt, R. G. 2004, *ApJS*, 152, 211
- Chapman, S. C., et al. 2000, *MNRAS*, 319, 318
- Rigopoulou, D., et al. 2006, *ApJ*, 648, 81
- Shim, H., Im, M., Choi, P., Yan, L., & Storrie-Lombardi, L. 2007, *ApJ*, 669, 749
- Kennicutt, Jr., R. C. 1998, *ARA&A*, 36, 189
- Pettini, M., Rix, S. A., Steidel, C. C., Adelberger, K. L., Hunt, M. P., & Shapley, A. E. 2002, *ApJ*, 569, 742
- Seitz, S., Saglia, R. P., Bender, R., Hopp, U., Belloni, P., & Ziegler, B. 1998, *MNRAS*, 298, 945
- Riechers, D. A., Carilli, C. L., Walter, F., & Momjian, E. 2010, *ApJ*, 724, L153
- Chapman, S. C., & Casey, C. M. 2009, *MNRAS*, 398, 1615
- Chary, R., & Elbaz, D. 2001, *ApJ*, 556, 562
- Rigopoulou, D., et al. 2006, *ApJ*, 648, 81
- Daddi, E., Dannerbauer, H., Elbaz, D., Dickinson, M., Morrison, G., Stern, D., & Ravindranath, S. 2008, *ApJ*, 673, L21
- Elbaz, D., et al. 2007, *A&A*, 468, 33
- Lo Faro, B., et al. 2013, *ApJ*, 762, 108
- Rodighiero, G., et al. 2011, *ApJ*, 739, L40
- Kaviraj, S., et al. 2012, *MNRAS*, L26

Rowan-Robinson, M. 2012, in IAU Symposium, Vol. 284, IAU Symposium, ed. R. J. Tuffs & C. C. Popescu, 446–455

Takagi, T., Arimoto, N., & Hanami, H. 2003, MNRAS, 340, 813

Siebenmorgen, R., & Krügel, E. 2007, A&A, 461, 445

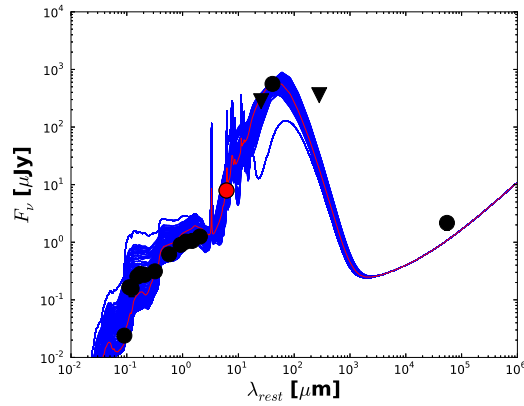


Fig. 5.— Rest-frame SEDs of a $10^{11}M_{\odot}$ galaxy at 0.5 Gyr with various dust environments and dust intrinsic properties. Blue lines: various dust size distributions and MC properties. Only with these various properties, the UV-optical part of the SED varies by a factor of ten. It is clear that the MW properties cannot fit the SED. Red line: MW dust and MC properties in Table 3 and Table 4. MIPS-LBGs data are from Magdis et al. (2010b) as described in Fig 3.

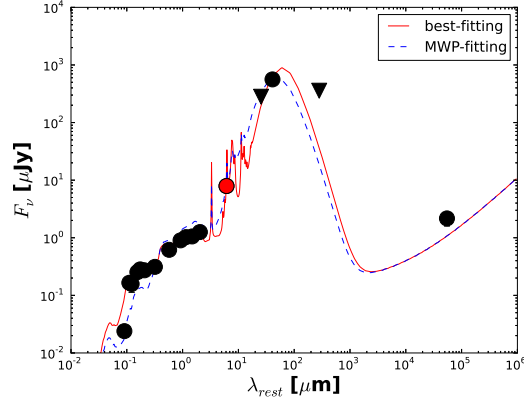


Fig. 6.— “Best-fitting” rest-frame SED. Red solid line: the “best-fitting” SED of a $10^{11} M_{\odot}$ galaxy at 0.5 Gyr with MIPS-LBGs dust and MC properties shown in Table 3 and Table 4. At the third fitting step, this “best-fitting” model is given by min- χ^2 fitting approach based on the grid models shown in Fig. 5. The values in Table 3 and Table 4 just give the general properties of the dust and MCs and should not be considered as the real ones. Note that, one can get an another “best-fitting” model using another galaxy model (such as a $10^{11} M_{\odot}$ galaxy at 0.4 Gyr). However, the overall-level SEDs are similar for models within a small age parameter space (see Fig. 4). Therefore, the trend of the dust and MC properties is the same for those models with different age. However, the parameters of Milky Way can not fit the SED no matter what the galactic age is adopted (see examples in Fig. 4). The mean differences between the “best-fitting” and “Milky Way parameters-fitting” SED (Blue dashed line, “WMP-fitting”) are the UV-optical shape and the position of the FIR peak. MIPS-LBGs data are from Magdis et al. (2010b) as described in Fig 3.

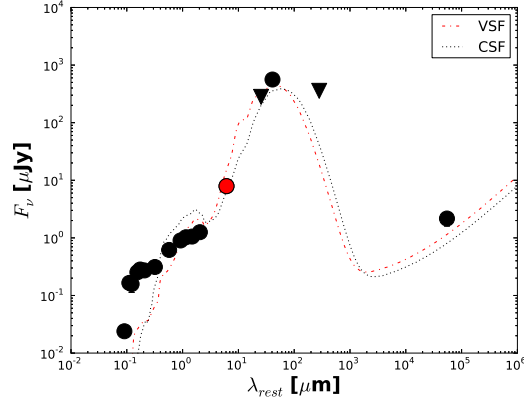


Fig. 7.— Rest-frame SEDs of different models. To show the necessary of more reliable SFHs, SEDs of a model (age ~ 0.5 Gyr, stellar mass $\sim 8 \times 10^{10} M_{\odot}$), which takes a self-consistent SFH (M11 case in Fig. 1, SSF for short) and a model (age ~ 2 Gyr, stellar mass $\sim 9 \times 10^{10} M_{\odot}$) with a constant SFH (CSF) are shown. MIPS-LBGs data are from Magdis et al. (2010b) as described in Fig 3.

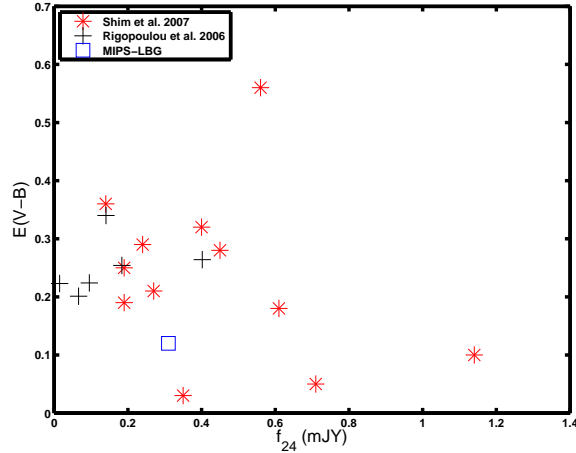


Fig. 8.— Observed $24 \mu\text{m}$ flux density f_{24} vs estimated extinction $E(B-V)$ for $24\mu\text{m}$ MIPS detected LBGs at $z \sim 3$. Asterisk, cross, square symbols represent data from Shim et al. (2007), Rigopoulou et al. (2006) and the average MIPS-LBG, respectively. The f_{24} is not correlated with $E(B-V)$ for these objects.

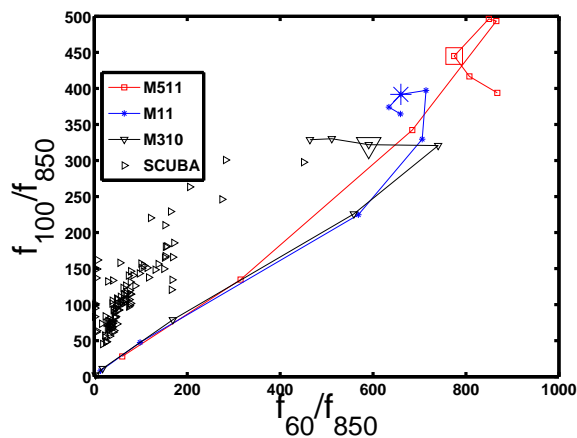


Fig. 9.— Rest-frame f_{100}/f_{850} flux density ratio vs f_{60}/f_{850} flux density ratio. The data of SCUBA local galaxies are from Dunne et al. (2000). Lines are our model predictions of f_{100}/f_{850} vs f_{60}/f_{850} evolution from 0.1 to 0.7 Gyr. The large triangle, asterisk and square are corresponding for M310, M11 and M510 model predictions at 0.5Gyr, respectively. The high redshift galaxies and local SMGs have different FIR properties.